Volume 56
Number 70
11 September 2020
Pages 10087–10260

ChemComm

Chemical Communications

rsc.li/chemcomm

ISSN 1359-7345

ROYAL SOCIETY OF CHEMISTRY

COMMUNICATION

Gregory C. Welch, Clément Cabanetos *et al.*
Synthesis, characterization and use of benzothioxanthene imide based dimers

ChemComm

COMMUNICATION

View Article Online
View Journal | View Issue

Cite this: *Chem. Commun.*, 2020, **56**, 10131

Received 2nd July 2020,
Accepted 10th August 2020

DOI: 10.1039/d0cc04556j

rsc.li/chemcomm

Synthesis, characterization and use of benzothioxanthene imide based dimers†

José María Andrés Castán,‡[a] Clément Dalinot,‡[a] Sergey Dayneko,[b] Laura Abad Galan,[c] Pablo Simón Marqués,[a] Olivier Alévêque,[a] Magali Allain,[a] Olivier Maury,[c] Ludovic Favereau,[d] Philippe Blanchard,[a] Gregory C. Welch *[b] and Clément Cabanetos *[a]

The synthesis of benzothioxanthene imide based dimers is reported herein. Subtle chemical modifications were carried out and their impact on the optical and electrochemical properties was investigated for a better structure–property relationship analysis. The icing on the cake was that these new structures were used as light emitting materials for the fabrication and demonstration of the first BTXI-based OLEDs.

Over the years, imide containing rylenes have demonstrated their potential as strong candidates for a variety of organic electronic applications due to their excellent thermal, chemical and photochemical stabilities, as well as intriguing electronic and redox properties.[1] Perylene and naphthalene diimides can be clearly identified as the beacons of this molecular family in terms of reported studies, chemical modifications and target applications (Fig. 1).[2]

Motivated by the exploration and functionalization of original chemical structures, we have recently focused our attention on an overlooked and inexpensive vat dye, benzothioxanthene imide (**BTXI**). Never used for organic electronic purposes and exclusively functionalized on the nitrogen atom of the imide group, we have reported the selective and efficient monobromination of its rylene core, affording **BTXI-Br** (Fig. 1),[3,4] and have opened the door to the design of new and original molecular architectures that have been successfully evaluated as active materials in organic photovoltaic (OPV) devices.[5,6] Consequently, to further explore the potential of this dye, we report herein the synthesis and use of three dimers to prepare the first **BTXI**-based organic light-emitting diodes (OLEDs).

As depicted in Scheme 1, target molecules stemmed from the common **BTXI-Br** derivative. The later was indeed either sulfonated (**BTXI-SO$_2$-Br**) or engaged in a Suzuki–Miyaura cross-coupling reaction in order to be subsequently and efficiently mono-brominated at the bay position (**Br-BTXI**).

Finally, dimers **D1**, **D2** and **D3** were prepared from the corresponding bromo derivatives, namely **BTXI-Br**, **BTXI-SO$_2$-Br** and **Br-BTXI,** respectively, under copper-catalyzed Ullmann reaction conditions.[7] In parallel, pallado-catalyzed cross-coupling conditions have been applied, in a further attempt to improve the synthetic yields, particularly for **D1** and **D3**, but were not found to be very convincing (Scheme S1, ESI†).

Single crystals of all the dimers were prepared by slow evaporation techniques. In addition to confirming the structures, the latter highlighted, as expected, large dihedral angles between the constituting **BTXI** units of *ca.* 75.9, 75.6 and 60.2 for **D1**, **D2** and **D3,** respectively (Fig. 2). Such important twists might contribute to the good solubility of the derivatives and should profoundly modify the self-assembly properties compared to those of the **BTXI** monomer, and consequently tune the solid-state luminescence (*vide supra*). Comparison of crystal packing indicates that (i) **BTXI** forms a very regular head-to-tail stacking with strong cofacial π-interactions (d = 3.675 and 3.816 Å, Fig. S20, ESI†); (ii) **D1** and **D2** crystallized

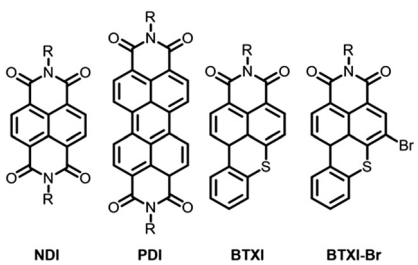

Fig. 1 Structure of **NDI**, **PDI**, **BTXI** and **BTXI-Br**.

[a] *CNRS UMR 6200, MOLTECH-Anjou, University of Angers, 2 Bd Lavoisier, 49045 Angers, France. E-mail: clement.cabanetos@univ-angers.fr*
[b] *Department of Chemistry, University of Calgary, 2500 University Drive N.W., Calgary, Alberta T2N 1N4, Canada*
[c] *Univ Lyon, ENS de Lyon, CNRS UMR 5182, Université Claude Bernard Lyon 1, F-69342 Lyon, France*
[d] *Univ Rennes, CNRS, ISCR – UMR 6226, ScanMAT – UMS 2001, F-35000 Rennes, France*

† Electronic supplementary information (ESI) available. CCDC 2012963 and 2012965–2012967. For ESI and crystallographic data in CIF or other electronic format see DOI: 10.1039/d0cc04556j

‡ Both authors equally contributed to this work.

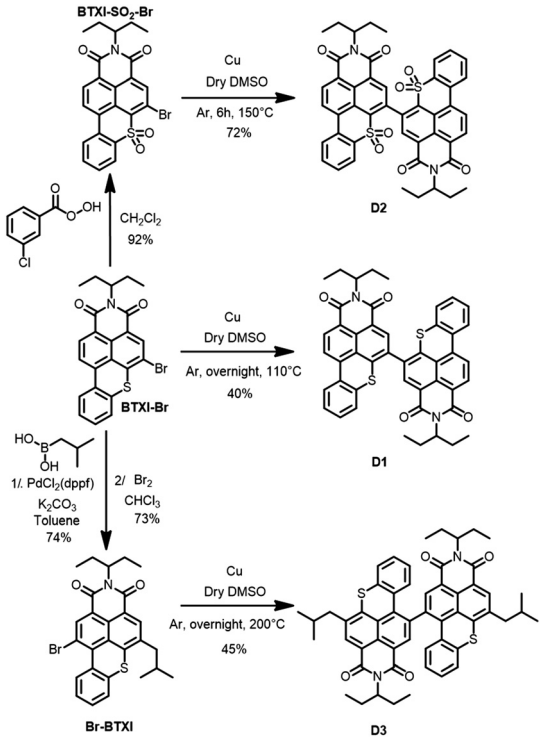

Scheme 1 Synthetic route to **D1**, **D2** and **D3**.

as dimers with strong and moderate intermolecular π-interactions, respectively (Fig. S21 and S22, ESI†); and **D3** forms a more complex hexameric toroidal structure with circular slipped π-interactions between two vicinal molecules (Fig. S23–S25, ESI†).

In parallel, the photophysical properties have been investigated in both diluted dichloromethane solution and in the solid state. The results are listed in Table 1. In solution, it appears that oxidation into sulfones (**D2**) induces a significant blue shift (of *ca.* 50 nm) of the long-wavelength absorption band (π–π* transitions) initially centered around 450 nm (**D1**, **D3**) (Fig. S16 and S28, ESI†), in agreement with the previously reported **BTXI**-SO_2 derivative.[8] A similar effect is also observed in the emission. Importantly, compared to **BTXI**,[8] the dimerization results in a significant decrease of the luminescence quantum yield in solution (Table 1). This effect is explained by a more favoured intersystem crossing process of a non-emissive triplet state (note that a detailed photophysical study will be published elsewhere). When moving to the solid state, the photophysics of the compounds are governed by the present intermolecular interactions. For instance, the emission of **BTXI** is red shifted and completely quenched due to aggregation quenching as a result of the formation of the strong π-stacking intermolecular interactions described above (Fig. S20, ESI†). This observation is also valid for dimer **D1** with only a 0.06 quantum yield. **D2** shows a larger quantum yield of 0.14 that can be explained by the distortion induced by the sulphur oxidation reducing the π-stacking intermolecular interactions. Finally, **D3** presents a sharp emission at 580 nm strongly red-shifted (FWHM = 1442 cm^{-1} against 2348 cm^{-1} and 3145 cm^{-1} for **D1** and **D2**, respectively), accompanied by the highest quantum yield of the series. This behaviour is

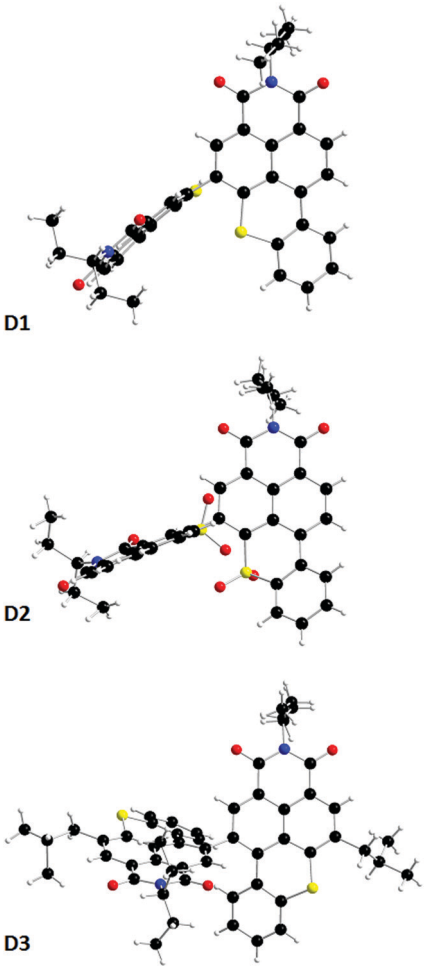

Fig. 2 X-ray structures of **D1**, **D2** and **D3**.

in agreement with the slipped π-interactions observed in the crystal structure and suggests the formation of J-aggregates in the solid state that are frequently observed for the perylene diimide chromophore family (Fig. 3).[9]

The cyclic voltammogram of **D1**, plotted in Fig. 4, revealed the presence of two reversible and successive processes in both the positive and negative regions attributed to the formation of stable cation/di-cation and anion/di-anion species, respectively.

While changing the grafting position (**D3**) induces a more visible splitting of the reversible processes with minor impact on their potentials (greater delocalization of charges), the conversion of the sulfurs into sulfones results in a drastic modification of the electrochemical signatures of **D2**. Indeed, on one side, the reversibility of the oxidation processes seems to be lost, while on the other side, two reversible and quasi-reversible split waves were recorded in the negative region. Thereafter, frontier molecular orbital energy levels were thus estimated from the onset of the first oxidation and reduction waves (Table 1). With almost similar LUMO levels, dimerization in the bay area (**D3** *vs.* **D1**) induces a slight destabilization of the HOMO level resulting in the reduction of the gap also highlighted during the UV-visible measurements. In stark contrast, oxidation of the sulfur into sulfone causes the stabilization of

Table 1 Optical and electrochemical data recorded for **D1**, **D2** and **D3**

Dimer	λ_{abs} (nm)	ε (M^{-1} cm^{-1})	λ_{em} (nm)	$\Phi_f{}^a$	$\lambda_{em}{}^b$ (nm)	$\Phi_f{}^b$	E_{pa} ($V_{Fc+/Fc}$)	E_{pc} ($V_{Fc+/Fc}$)	E_{HOMO} (eV)	E_{LUMO} (eV)	ΔE_{elec} (eV)
BTXI	455	22 000	502	0.99	579	0.02	0.94	−1.82	−5.63	−3.10	2.53
D1	455	51 000	509	0.19	534	0.06	1.00	−1.74	−5.64	−3.16	2.48
D2	384	37 000	450	0.29	460	0.14	1.47	−1.18	−6.07	−3.73	2.35
D3	473	31 000	530	0.34	580	0.18	0.86	−1.70	−5.54	−3.21	2.32

[a] In solution. [b] On powders.

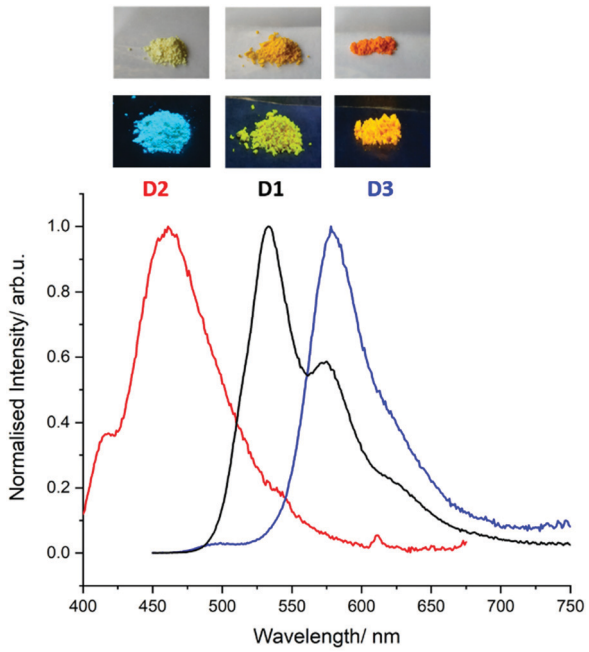

Fig. 3 Photograph of powders of **D1**, **D2** and **D3** under white light (top) and 254 nm (bottom) and their respective emission spectra.

both frontier orbitals while increasing the band gap. Complementarily investigated by computational chemistry, simulated frontier energy levels and UV-visible spectra were also found to follow these experimental trends (Fig. S26–S28 and Table S2, ESI†).

Hence, and as a further step into the characterization of these dimers and for a deeper structure–property relationship investigation, solution-processed OLED devices, of architecture: glass/ITO/PEDOT:PSS/emitting layer (EML)/ZnO/Ag, were then fabricated.[10] The luminescent and commercially available conjugated polymer PFO, also known as **F8**, was used in the EMLs as a host material to improve the performances of small molecule-based OLEDs.[10,11]

Tested under ambient conditions, it is noteworthy that all devices emitted light when connected to an external voltage, thus demonstrating, for the first time, up and running **BTXI**-based OLEDs. An overview of the main characteristics of the three **BTXI**-based OLEDs is summarized in Table 2 and their electroluminescence spectra (EL) and the Commission Internationale de l'Eclairage (CIE) color coordinates are shown in Fig. 5. In agreement with the optical properties of the three dimers, different colors of emitted lights, from blue to orange, were recorded. These results highlight, once again, the ease of

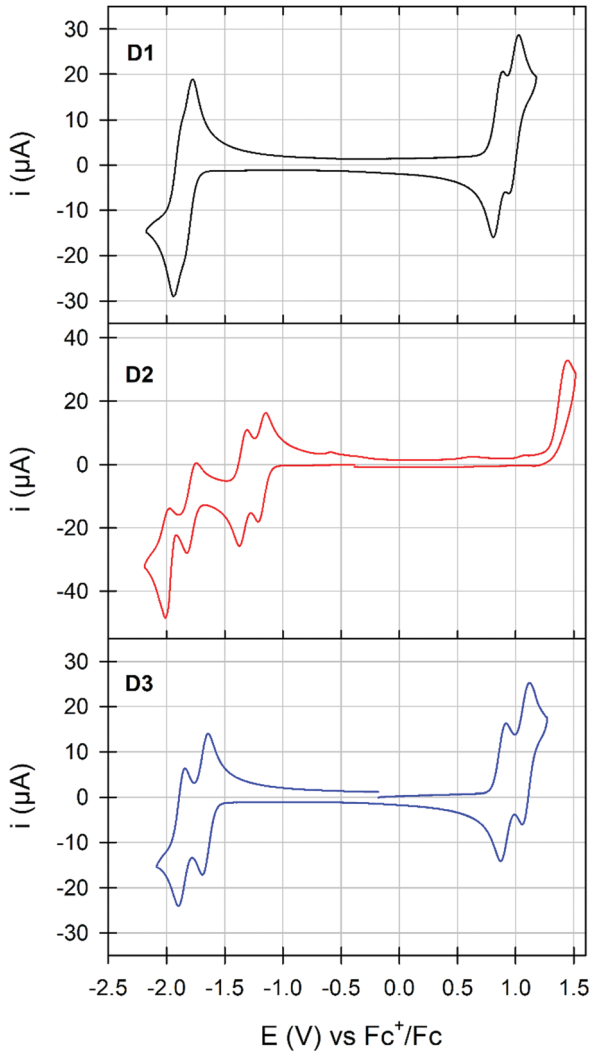

Fig. 4 Cyclic voltammogram of **D1** (top), **D2** (middle) and **D3** (bottom).

Table 2 OLED performance based on PFO and/or blends with dimers

Emitting layer	Ratio	V_{on} (V)	EQE_{max} (%)	LE_{max} (cd A^{-1})	PE_{max} (lm W^{-1})	L_{max} (cd m^{-2})
PFO:**D1**	2 : 18	4.8	0.04	0.26	0.30	608 (@9.9 V)
PFO:**D2**	2 : 18	3.9	0.04	0.08	0.04	1336 (@6.9 V)
PFO:**D3**	2 : 18	3.9	0.17	0.37	0.16	2860 (@10 V)

tunability at different levels induced by simple chemical modifications. The redshift and changing of EL shape of **BTXI**-based OLEDs relative to the photoluminescence is a result of the

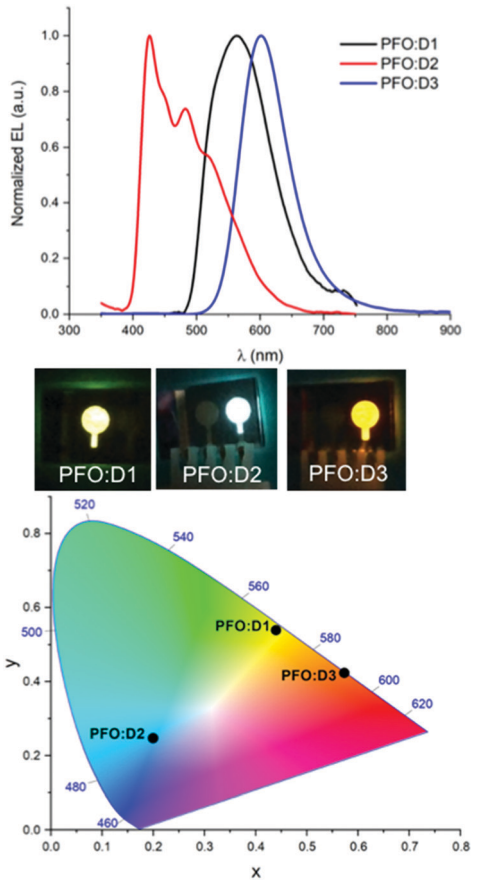

Fig. 5 Electroluminescence spectra (top) and CIE color coordinate spectra (above) of the **D1** (black), **D2** (red) and **D3** (blue) based devices under an external voltage.

aggregation of the dimers and various formation and relaxation of exciton mechanisms in the OLED structure (under voltage) and "clean" films (under light excitation).

In addition, the EML layers were spin-casted from *o*-xylene, which indicates that these materials can be easily transferred to develop flexible OLEDs by roll-to-roll coating into industrial scale. Moreover, the performance of these **BTXI**-based OLEDs could be improved by using a multilayer OLED structure.[12]

The synthesis and characterization of three original **BTXI**-based dimers is reported herein. Subtle chemical modifications, namely the oxidation of the constituting sulphur into sulfone and the dimerization in the bay area, were investigated as well as their impact on the optical and electrochemical properties. Due to their good solubility and highly twisted structures, these dimers were finally and successfully used as emitting materials for the demonstration of the first **BTXI**-based OLEDs.

JMA: synthesis, characterization and writing of the ESI, CD: synthesis and characterization, SD: device fabrication and testing, LAG and PSM: computational chemistry, OA: electrochemical characterization, MA: crystallographic characterization, OM: LAG's PI and discussions, PB, JMA/PSM's co-PI and discussions, GW: SD's PI and discussions, CC: CD's PI and JMA/PSM's co-PI, writing of the article.

The authors thank the MATRIX SFR of the University of Angers. J. M. A. C. and P. S. M. thank the European Union's Horizon 2020 research and innovation program under Marie Sklodowska Curie Grant agreement No. 722651 (SEPOMO). The *Région Pays de la Loire* is also acknowledged for the grant of C. D. (Projet étoile montante SAMOA). The authors are also grateful to ANR (SADAM ANR-16-CE07-0015-01) for the financial support and PDF grant of L. A. G. S. D. thanks the MITACS program for financial support. G. C. W. thanks the University of Calgary.

Conflicts of interest

There are no conflicts to declare.

Notes and references

1 T. Weil, T. Vosch, J. Hofkens, K. Peneva and K. Müllen, *Angew. Chem., Int. Ed.*, 2010, **49**, 9068–9093.
2 F. Würthner, C. R. Saha-Möller, B. Fimmel, S. Ogi, P. Leowanawat and D. Schmidt, *Chem. Rev.*, 2016, **116**, 962–1052.
3 P. Josse, S. Li, S. Dayneko, D. Joly, A. Labrunie, S. Dabos-Seignon, M. Allain, B. Siegler, R. Demadrille, G. C. Welch, C. Risko, P. Blanchard and C. Cabanetos, *J. Mater. Chem. C*, 2018, **6**, 761–766.
4 C. Dalinot, P. Simón Marqués, J. M. Andrés Castán, P. Josse, M. Allain, L. Abad Galán, C. Monnereau, O. Maury, P. Blanchard and C. Cabanetos, *Eur. J. Org. Chem.*, 2020, 2140–2145.
5 S. V. Dayneko, A. D. Hendsbee, J. R. Cann, C. Cabanetos and G. C. Welch, *New J. Chem.*, 2019, **43**, 10442–10448.
6 A.-J. Payne, N. A. Rice, S. M. McAfee, S. Li, P. Josse, C. Cabanetos, C. Risko, B. H. Lessard and G. C. Welch, *ACS Appl. Energy Mater.*, 2018, **1**, 4906–4916.
7 A. D. Hendsbee, J.-P. Sun, W. K. Law, H. Yan, I. G. Hill, D. M. Spasyuk and G. C. Welch, *Chem. Mater.*, 2016, **28**, 7098–7109.
8 L. A. Galán, J. M. Andrés Castán, C. Dalinot, P. S. Marqués, P. Blanchard, O. Maury, C. Cabanetos, T. Le Bahers and C. Monnereau, *Phys. Chem. Chem. Phys.*, 2020, **22**, 12373–12381.
9 S. Herbst, B. Soberats, P. Leowanawat, M. Stolte, M. Lehmann and F. Würthner, *Nat. Commun.*, 2018, **9**, 2646.
10 S. V. Dayneko, M. Rahmati, M. Pahlevani and G. C. Welch, *J. Mater. Chem. C*, 2020, **8**, 2314–2319.
11 J. H. Ahn, C. Wang, I. F. Perepichka, M. R. Bryce and M. C. Petty, *J. Mater. Chem.*, 2007, **17**, 2996–3001.
12 M. Rahmati, S. V. Dayneko, M. Pahlevani and G. C. Welch, *ACS Appl. Electron. Mater.*, 2020, **2**, 48–55.

